

SUPPORTING INFORMATION

Boosted Zn²⁺ Storage Performance of Hydrated Vanadium Oxide by Defect and Heterostructure

Viet Phuong Nguyen,^{a,b} Ji Su Park,^c Jong Min Yuk,^c Minsub Oh,^b Jae-Hyun Kim,^{a,b} Seung-Mo
Lee^{a,b,*}

^a Nanomechatronics, Korea University of Science and Technology (UST), Daejeon 34113,
Republic of Korea

^b Department of Nanomechanics, Korea Institute of Machinery and Materials (KIMM), Daejeon
34103, Republic of Korea

^c Department of Materials Science and Engineering, Korea Advanced Institute of Science and
Technology (KAIST), 335 Science Road, Daejeon 34141, Republic of Korea

* Corresponding author: sm.lee@kimm.re.kr

1. Experimental section

Preparation of d-VOH@CT

The d-VOH@CT heterostructure was synthesized by the natural oxidation effect. First, the natural cotton textile (TX304, TexWipe) was coated by a V₂O₅ layer using the atomic layer deposition (ALD) method. Vanadium(V) oxytriisopropoxide (V(O)(OCH(CH₃)₂)₃, VTIP, Sigma-Aldrich) heated to 70 °C and H₂O were employed as precursors. The ALD process condition was optimized and set in the exposure mode with 1 s pulse, 20 s exposure, and 30 s purging of VTIP, followed by the same recipe for H₂O for each ALD cycle at a constant N₂ flow rate of 30 sccm. The temperature and pressure of the ALD chamber (S100, Savannah, Cambridge NanoTech Inc.) were set to 150 °C and ~0.1 Torr, respectively. The thickness of the V₂O₅ layer was controlled by the number of the ALD cycle. The growth rate of V₂O₅ on a reference Si

substrate was measured as 0.4 Å/cycle. Next, the V₂O₅-coated cotton textiles with various V₂O₅ thicknesses were annealed at 900 °C for 1 minute to obtain VC/V₂O₃@CT. Subsequently, the VC/V₂O₃@CT sample was exposed to the air at room conditions for the desired time. Among various samples, the one exposed to the air for 30 days showed the most noteworthy changes, which were denoted as d-VOH@CT and used for further characterizations.

Synthesis of VOH

VOH was prepared by hydrothermal method. Briefly, 3 mmol V₂O₅ was dissolved into the mixture of 30 ml deionized water and 1 ml hydrogen peroxide to form an orange solution. Subsequently, 1 ml anhydrous ethanol was added to the orange solution. The solution was transferred into a 50 ml Teflon-lined stainless-steel autoclave and maintained at 160 °C for 5 h. After cooling down to room temperature naturally, the product was collected and washed with deionized water and dried in a vacuum at room temperature overnight.

Material characterization

SEM (JSM-7800F, JEOL) equipped with energy-dispersive x-ray spectroscopy (EDX) (Oxford AZtec® EDX system) was used to investigate the analysis of the morphology and the element. TEM (JEM-ARM200F, JEOL) was employed to characterize the microstructure of samples. XRD spectra were collected using an Empyrean diffractometer (PANalytical with Cu K α (λ = 1.5418 Å)). The FTIR spectra were obtained with a Nicolet 6700 FTIR spectrometer. X-ray photoelectron spectroscopy was performed using MultiLab 2000 (Thermo Fisher Scientific with an Al K α X-ray source). Thermogravimetric analysis (TGA) was conducted on a Shimadzu TGA-50 instrument in the air under a temperature ramping rate of 10 °C min⁻¹ from room temperature to 500 °C.

Electrochemical measurements:

The d-VOH@CT heterostructure was directly used as the binder-free cathode. In the case of VOH, it was mixed with carbon and polyvinylidene fluoride in a ratio of 7:2:1 with N-methyl-2-pyrrolidone, followed by grinding for at least 30 min to obtain a slurry. The slurry was then coated onto CT, which was prepared by removing d-VOH on d-VOH@CT by HCl, and dried at 80 °C overnight. Zn metal foil and glass fiber were used as anode and separator, respectively. A 2 M ZnSO₄ aqueous solution was used as the electrolyte. The cycling performance was evaluated using a Wonatech battery cycler with a voltage range from 0.2 to 1.6 V at room temperature. The coin cell was activated for three cycles at 0.1 A g⁻¹ before long-term cycling at 1.0 A g⁻¹ and 5.0 A g⁻¹. Electrochemical impedance spectroscopy (EIS) data were collected with an electrochemical workstation (VPS, Bio-Logic Science Instruments) in the frequency range of 100 kHz to 0.01 Hz. Specific capacity values were calculated based on the mass loading of the active materials. The mass of d-VOH in the d-VOH@CT heterostructure was determined by the weight difference of 1-cm² material before and after removing d-VOH by HCl (~2.06 mg cm⁻²).

Measurements of GITT

The GITT measurements were performed by repeatedly applying the current density of 0.1 A g⁻¹ for 20 min, followed by a 20-min rest step to reach the equilibrium until the voltage reached 0.2 V. The diffusion coefficients of Zn²⁺ ion were calculated from the obtained GITT curves using the following equation:

$$D = \frac{4l^2}{\pi\tau} \left(\frac{\Delta E_S}{\Delta E_t} \right)^2$$

where D , l , t , and τ are the diffusion coefficient, the Zn²⁺ diffusion length, the duration time of the current pulse, and the relaxation time, respectively. ΔE_S is the voltage change in the over cell voltage upon a current pulse, and ΔE_t is the voltage change among the last and current steady-state voltage.

2. Supporting figures

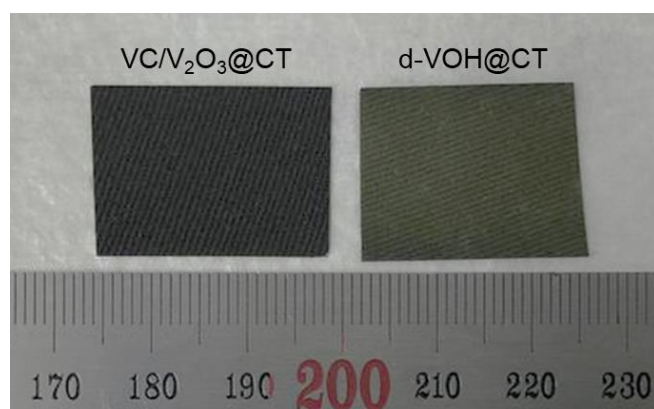


Figure S1. Digital photo of the VC/V₂O₃@CT and the d-VOH@CT.

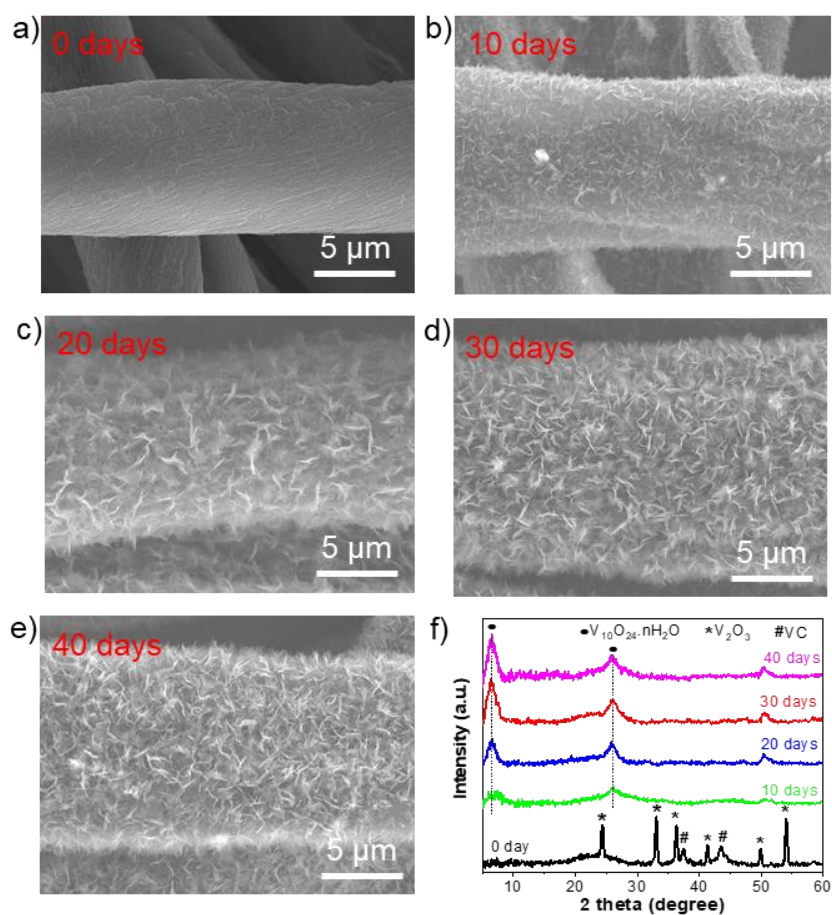


Figure S2. a-e) SEM images showing the morphology of samples exposed to air for 0 days, 10 days, 20 days, 30 days, and 40 days, respectively. f) Corresponding XRD patterns.

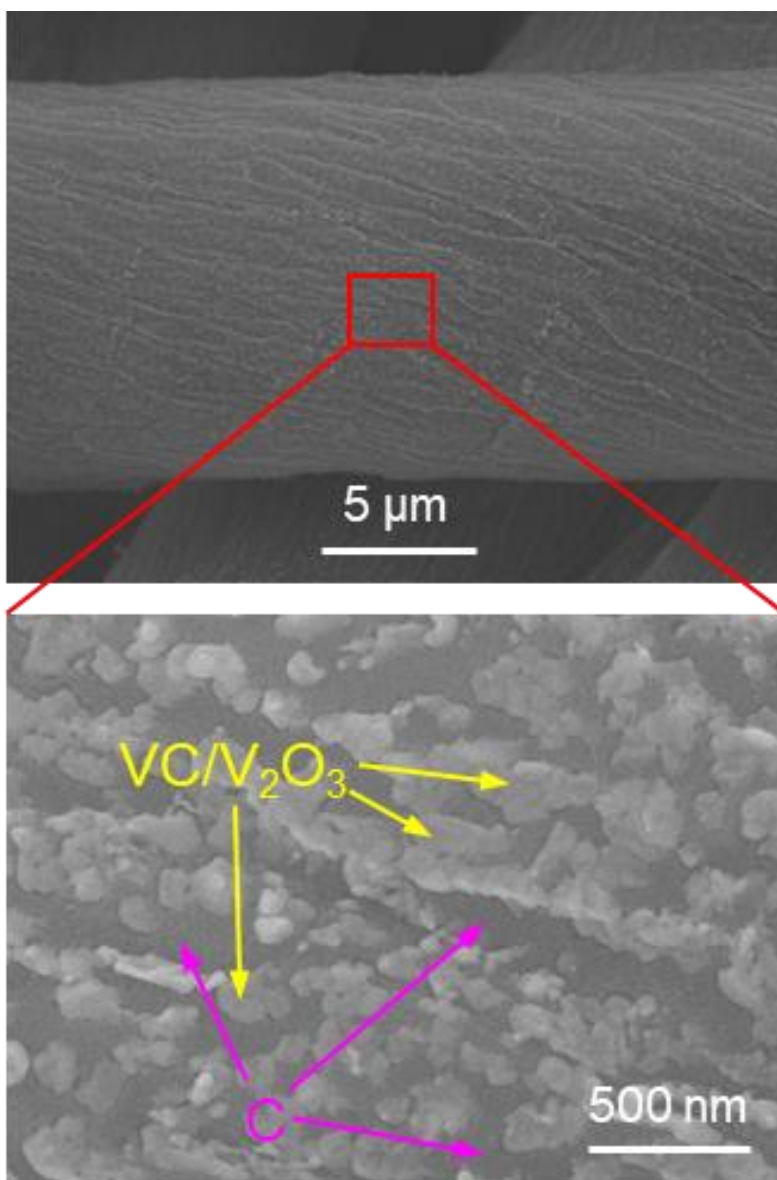


Figure S3. SEM images showing VC/V₂O₃ nanoparticles embedded in the porous CT. The sample was prepared by annealing the cotton textile coated with 10-nm V₂O₅.

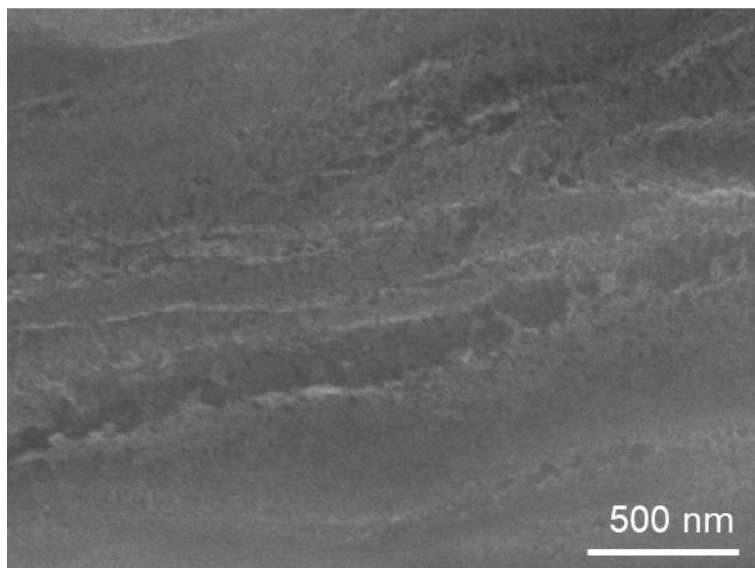
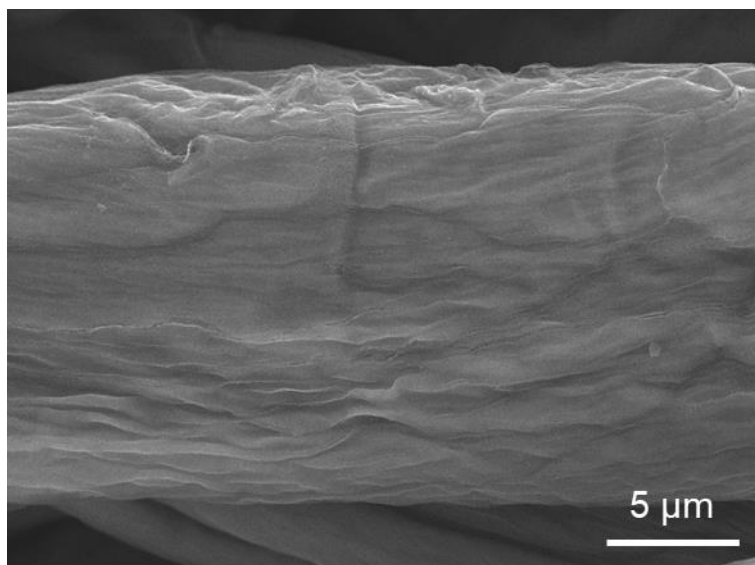


Figure S4. SEM image of porous CT after removing d-VOH.

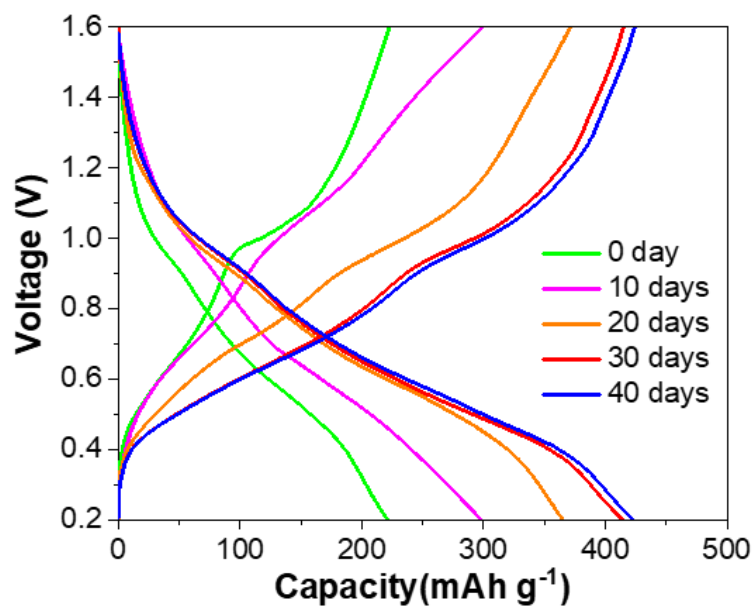


Figure S5. Representative galvanostatic discharge/charge profiles of the samples exposed to the air for 0 days, 10 days, 20 days, 30 days, and 40 days. The capacities of samples exposed to air for 30 and 40 days are similar, indicating the precursor materials are likely completely oxidized after 30 days.

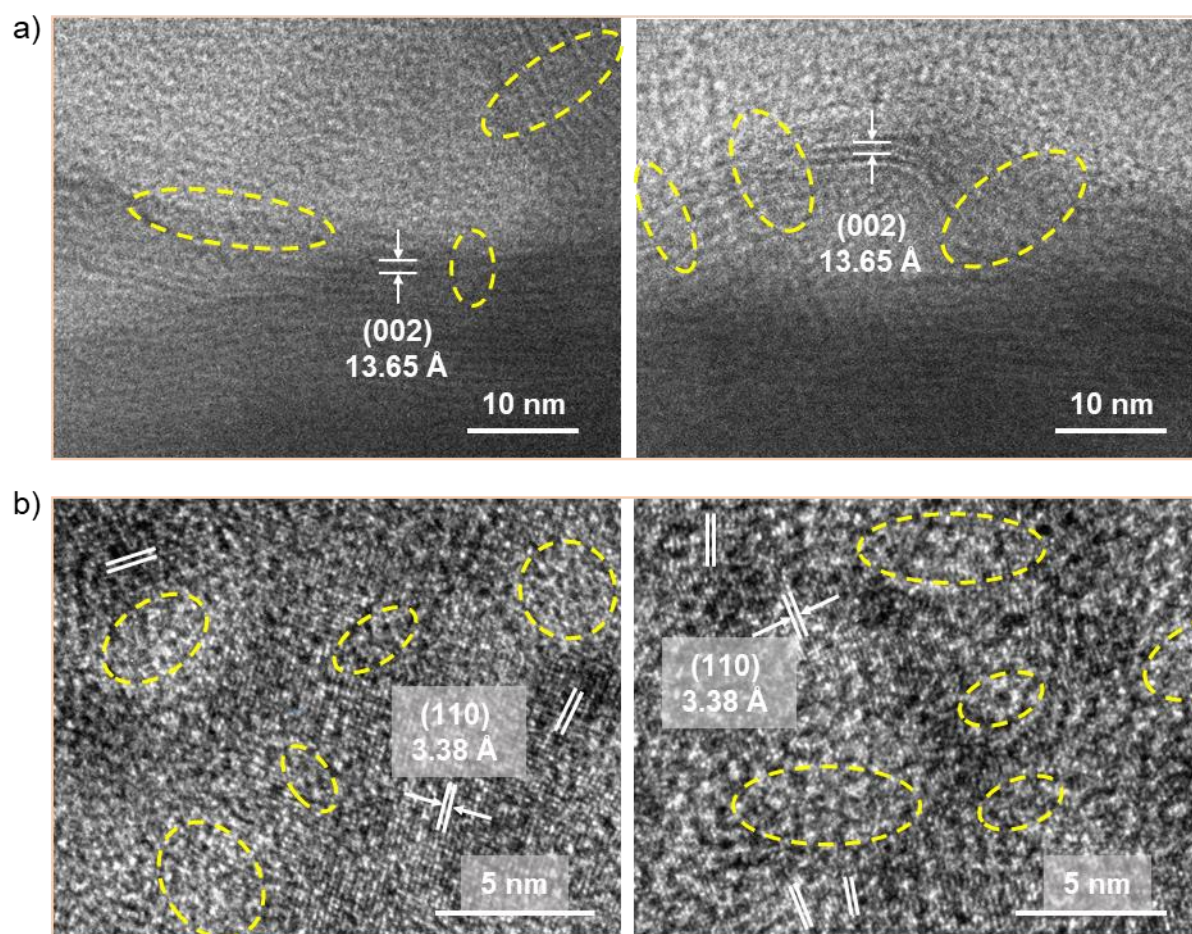


Figure S6. High-resolution TEM images showing (a) the interlayer spacing and (b) lattice distortion of d-VOH.

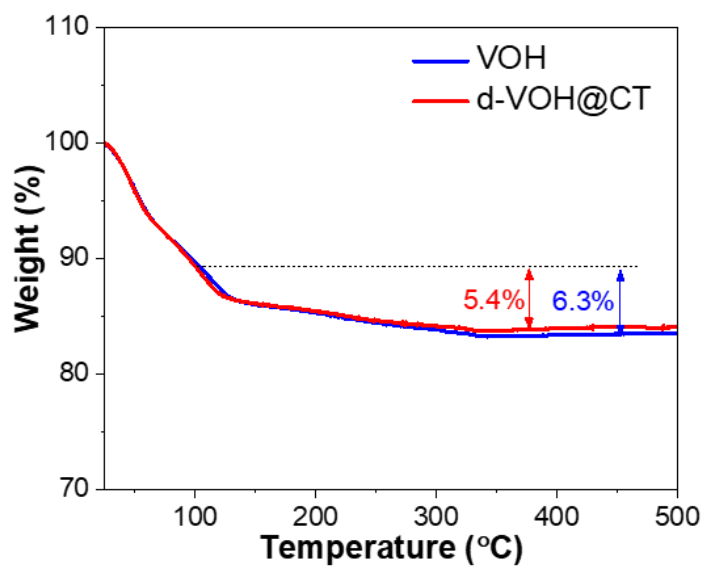


Figure S7. TGA curves of d-VOH@CT and VOH.

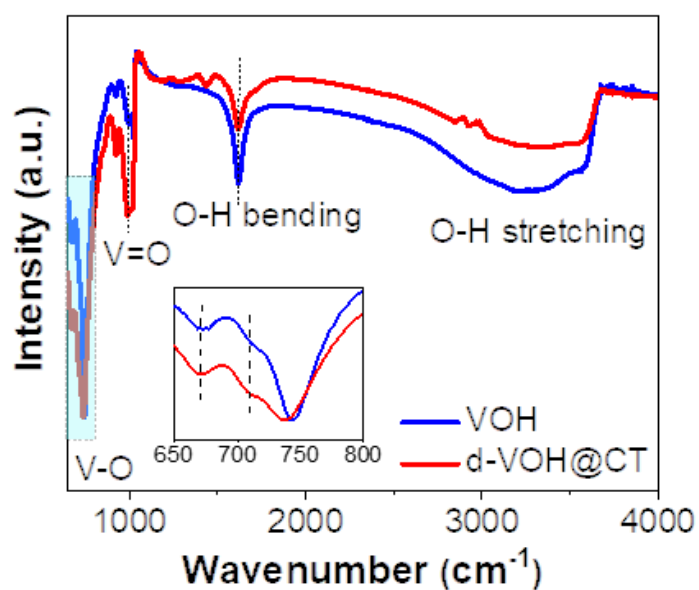


Figure S8. FTIR spectra of d-VOH@CT and VOH. The inset shows enlarged FTIR spectra at wavenumber from 650 to 800 cm^{-1} .

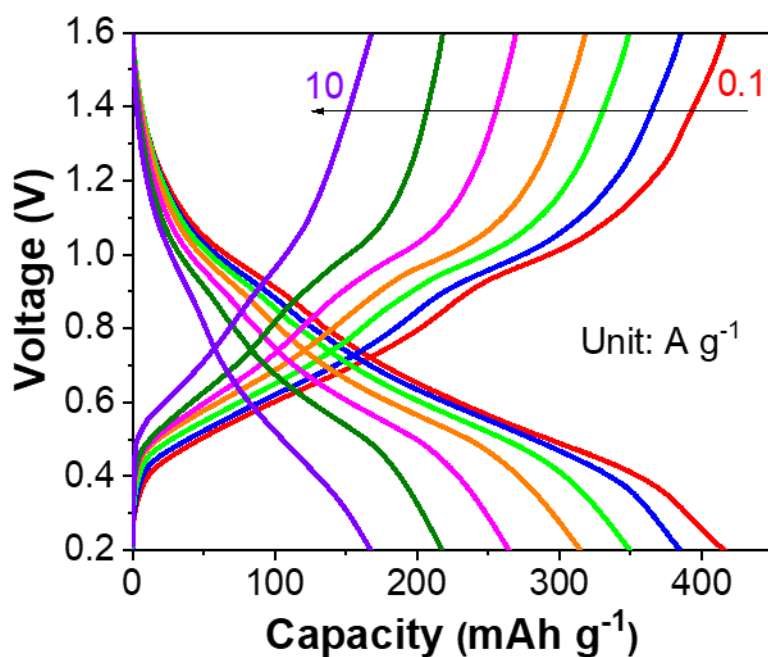


Figure S9. Galvanostatic discharge/charge profiles of the d-VOH@CT cathode at various current densities.

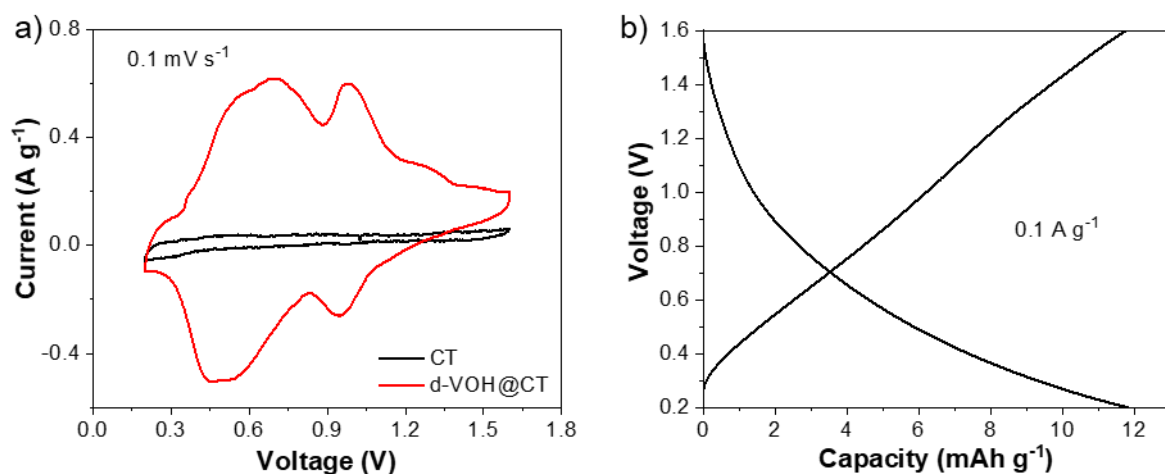


Figure S10. Capacity contribution of the CT. a) CV curves of CT and d-VOH@CT at 0.1 mV s^{-1} . b) Galvanostatic discharge/charge profiles of the CT cathode at the current density of 0.1 A g^{-1} .

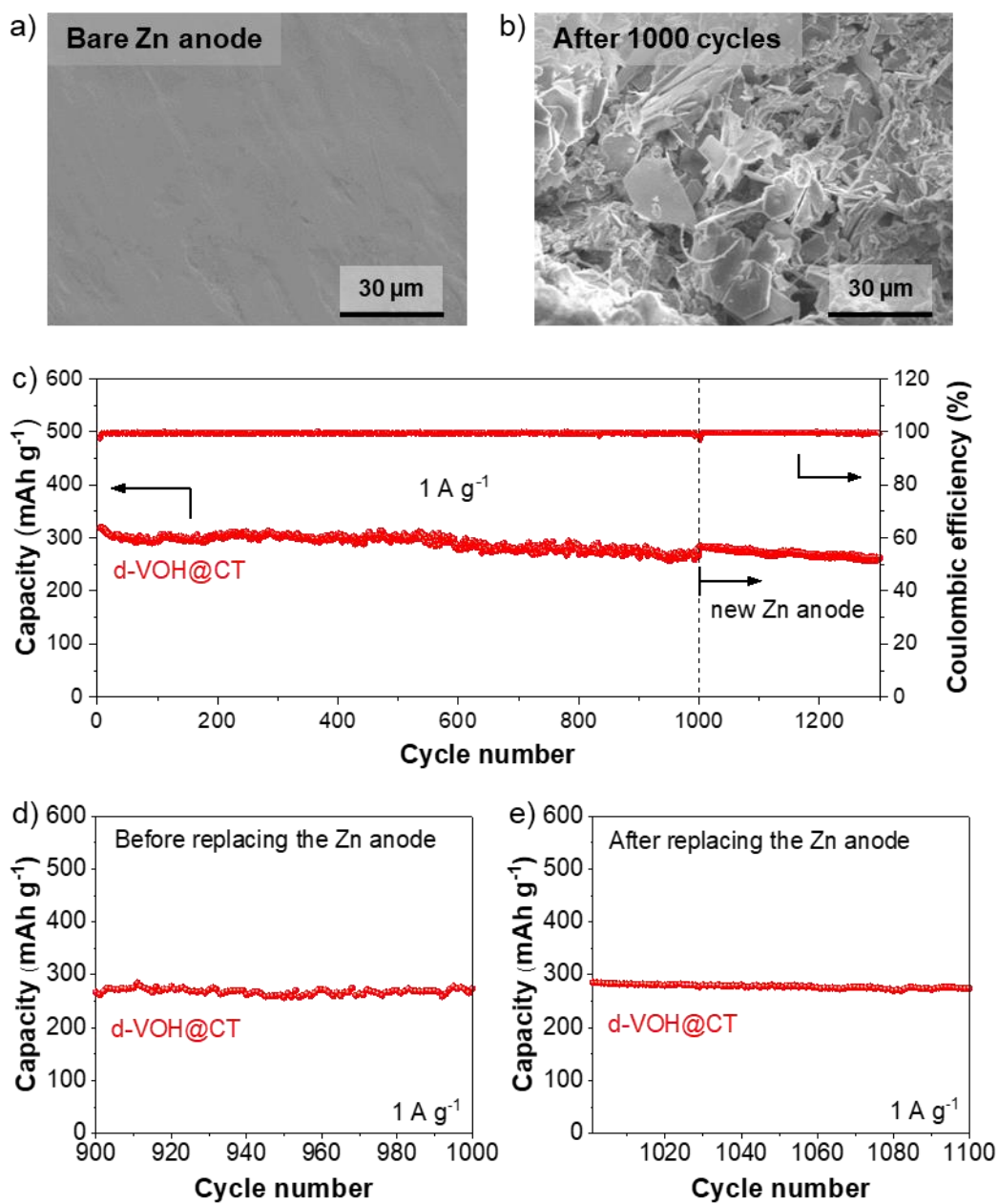


Figure S11. a-b) The morphology of the Zn anode before and after cycling. c) The change in the cycling performance of the d-VOH@CT after replacing the cycled Zn anode with a new Zn anode. d) Cycling performance of the d-VOH@CT from the 900th cycle to the 1000th cycle. e) Cycling performance of the d-VOH@CT from the 1001st cycle to the 1100th cycle.

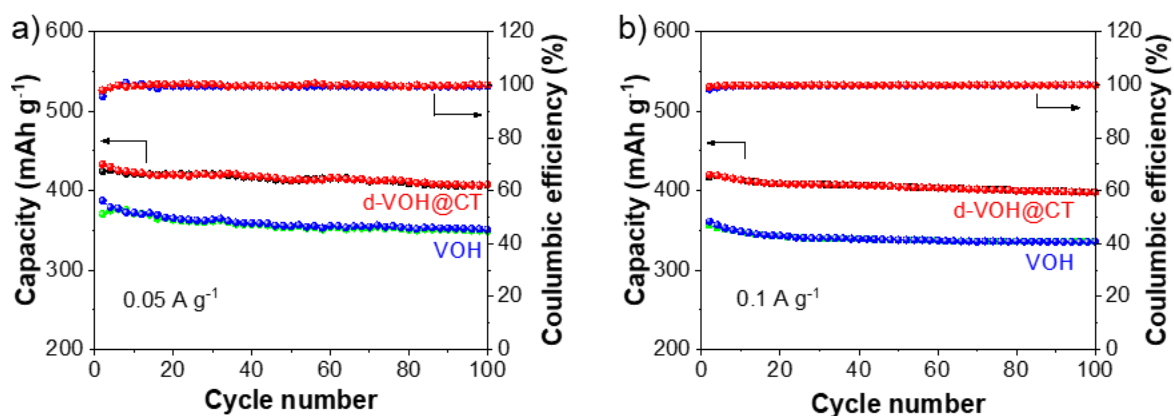


Figure S12. Cycling stability at (a) 0.05 A g⁻¹ and (b) 0.1 A g⁻¹ of the d-VOH@CT and VOH cathodes.

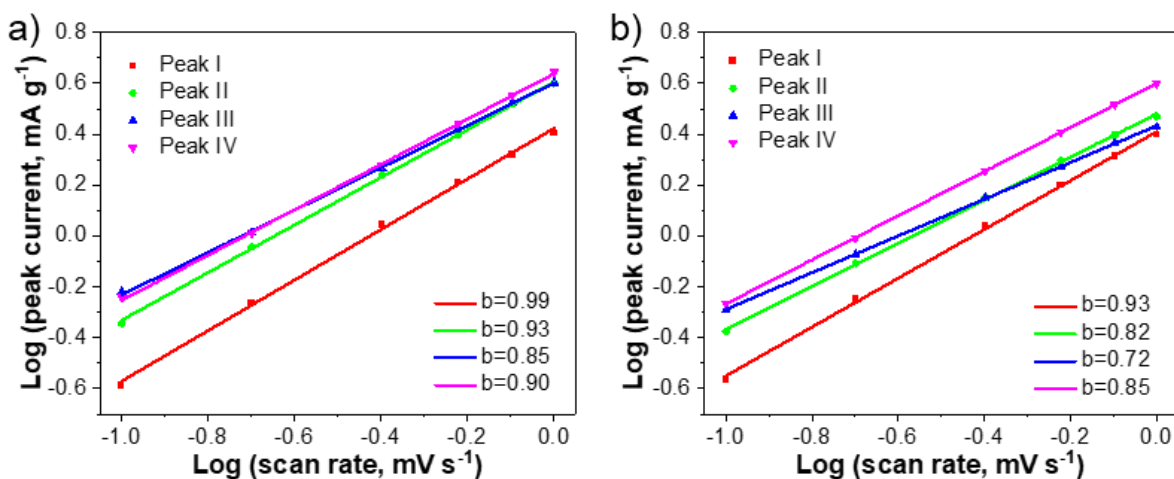


Figure S13. Plots of log (i) versus log (v) at specific peak currents extracted from the CV scans of (a) d-VOH@CT and (b) VOH.

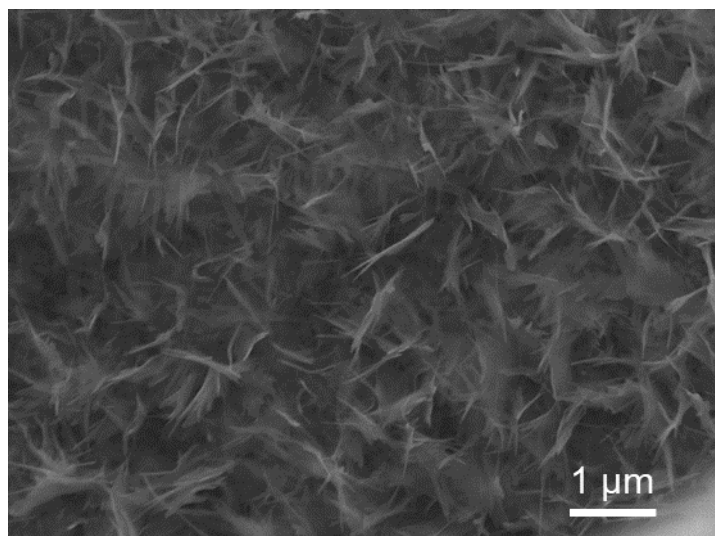


Figure S14. SEM image of d-VOH@CT after cycling.

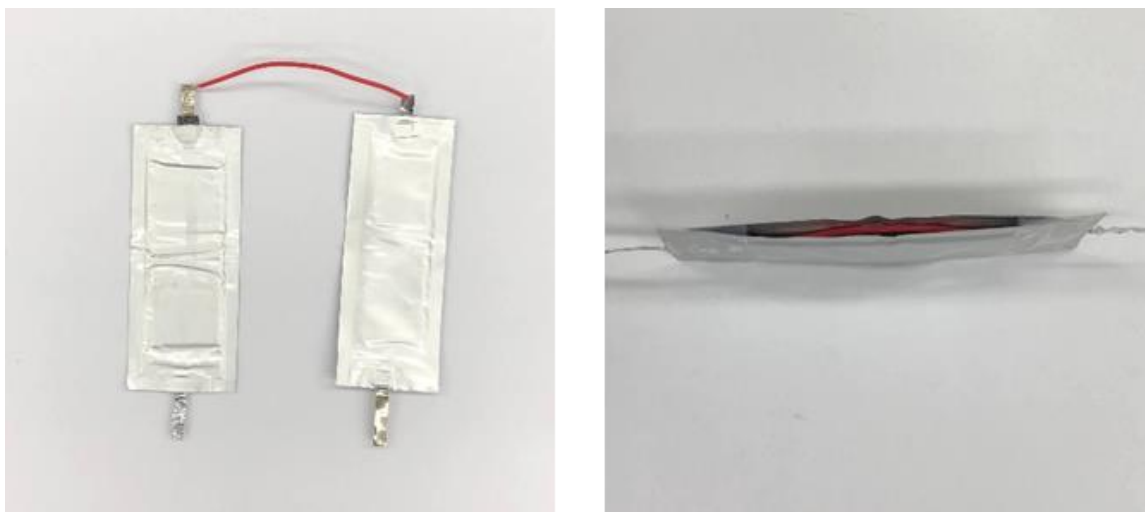


Figure S15. Digital photos of two flexible pouch cells in series.

Table S1. XRD analysis results of (002) peak.

Sample	2 θ (°)	Interlayer spacing (Å)	FWHM (2 θ)
d-VOH@CT	6.47	13.66	1.68
VOH	6.54	13.51	0.52

Table S2. Percentage of chemical state in the V element calculated from XPS spectra (unit: %).

Bond	VOH	d-VOH@CT
V ⁴⁺	15.1	27.3
V ⁵⁺	84.9	72.7

Table S3. Percentage of chemical state in the O element calculated from XPS spectra (unit: %).

Bond	VOH	d-VOH@CT
O-V	83.2	66.0
O-C	0	9.1
O _d	10.1	20.4
O-H	6.7	4.5

Table S4. Electrochemical performances of recently reported vanadium-based Zn-ion battery cathode materials.

Material	Specific capacity	Cycle performance	Ref.
Zn _{0.25} V ₂ O ₅ ·nH ₂ O	282 mAh g ⁻¹ at 0.3 A g ⁻¹ 183 mAh g ⁻¹ at 6 A g ⁻¹	80% retained after 1,000 cycles at 2.4 A g ⁻¹	1
Zn ₃ V ₂ O ₇ (OH) ₂ ·2H ₂ O	213 mAh g ⁻¹ at 0.05 A g ⁻¹ 54 mAh g ⁻¹ at 3 A g ⁻¹	68% retained after 300 cycles at 0.2 A g ⁻¹	2
α-Zn ₂ V ₂ O ₇	248 mAh g ⁻¹ at 0.05 A g ⁻¹ 170 mAh g ⁻¹ at 4.4 A g ⁻¹	85% retained after 1,000 cycles at 4 A g ⁻¹	3
O _d -VO	401 mAh g ⁻¹ at 0.2 A g ⁻¹ 279 mAh g ⁻¹ at 2 A g ⁻¹	86% retained after 2,000 cycles at 2 A g ⁻¹	4
H-VO ₂	414 mAh g ⁻¹ at 0.1 A g ⁻¹ 200 mAh g ⁻¹ at 5 A g ⁻¹	70% retained after 3,000 cycles at 5 A g ⁻¹	5
CO ₂ -V ₆ O ₁₃	471 mAh g ⁻¹ at 0.1 A g ⁻¹ 175 mAh g ⁻¹ at 10 A g ⁻¹	80% retained after 4,000 cycles at 2 A g ⁻¹	6
VO ₂	394 mAh g ⁻¹ at 0.1 A g ⁻¹ 178 mAh g ⁻¹ at 3 A g ⁻¹	81.2% retained after 1,200 cycles at 3 A g ⁻¹	7
Ag _x V ₃ O ₇ ·H ₂ O@rGO	437 mAh g ⁻¹ at 0.1 A g ⁻¹ 170 mAh g ⁻¹ at 2 A g ⁻¹	72% retained after 1,000 cycles at 2 A g ⁻¹	8
NaV ₃ O ₈ ·1.5H ₂ O	380 mAh g ⁻¹ at 0.1 A g ⁻¹ 165 mAh g ⁻¹ at 5 A g ⁻¹	82% retained after 1,000 cycles at 4 A g ⁻¹	9
C@V ₂ O ₅	362 mAh g ⁻¹ at 0.5 A g ⁻¹ 98 mAh g ⁻¹ at 5 A g ⁻¹	72% retained after 5,000 cycles at 0.5 A g ⁻¹	10
Cu _{0.95} V ₂ O ₅	318 mAh g ⁻¹ at 0.1 A g ⁻¹ 195 mAh g ⁻¹ at 5 A g ⁻¹	92% retained after 1,000 cycles at 5 A g ⁻¹	11
NH ₄ V ₄ O ₁₀ ·0.28H ₂ O	410 mAh g ⁻¹ at 0.2 A g ⁻¹ 112 mAh g ⁻¹ at 10 A g ⁻¹	76% retained after 500 cycles at 2 A g ⁻¹	12
porous V ₂ O ₅	371 mAh g ⁻¹ at 0.2 A g ⁻¹ 234 mAh g ⁻¹ at 5 A g ⁻¹	73% retained after 1,000 cycles at 2 A g ⁻¹	13
d-VOH@CT	416 mAh g⁻¹ at 0.1 A g⁻¹ 168 mAh g⁻¹ at 10 A g⁻¹	88% retained after 2,000 cycles at 5 A g⁻¹	This work

Reference

- (1) Kundu, D.; Adams, B. D.; Duffort, V.; Vajargah, S. H.; Nazar, L. F. A High-Capacity and Long-Life Aqueous Rechargeable Zinc Battery Using a Metal Oxide Intercalation Cathode. *Nat. Energy* **2016**, *1*, 16119.
- (2) Xia, C.; Guo, J.; Lei, Y.; Liang, H.; Zhao, C.; Alshareef, H. N. Rechargeable Aqueous Zinc-Ion Battery Based on Porous Framework Zinc Pyrovanadate Intercalation Cathode. *Adv. Mater.* **2018**, *30*, 1705580.
- (3) Sambandam, B.; Soundharajan, V.; Kim, S.; Alfaruqi, M. H.; Jo, J.; Kim, S.; Mathew, V.; Sun, Y.; Kim, J. Aqueous Rechargeable Zn-Ion Batteries: An Imperishable and High-Energy $Zn_2V_2O_7$ Nanowire Cathode through Intercalation Regulation. *J. Mater. Chem. A* **2018**, *6*, 3850-3856.
- (4) Liao, M.; Wang, J.; Ye, L.; Sun, H.; Wen, Y.; Wang, C.; Sun, X.; Wang, B.; Peng, H. A Deep-cycle Aqueous Zinc-Ion Battery Containing an Oxygen-Deficient Vanadium Oxide Cathode. *Angew. Chem. Int. Ed.* **2020**, *59*, 2273- 2278.
- (5) Zhu, K.; Wu, T.; Sun, S.; van den Bergh, W.; Stefik, M.; Huang, K. Synergistic H^+/Zn^{2+} Dual Ion Insertion Mechanism in High-capacity and Ultra-Stable Hydrated VO_2 Cathode for Aqueous Zn-ion Batteries. *Energy Storage Mater.* **2020**, *29*, 60-70.
- (6) Shi, W.; Yin, B.; Yang, Y.; Sullivan, M. B.; Wang, J.; Zhang, Y. W.; Yu, Z. G.; Lee, W. S. V.; Xue, J. Unravelling V_6O_{13} Diffusion Pathways via CO_2 Modification for High-Performance Zinc Ion Battery Cathode. *ACS Nano* **2021**, *15*, 1273-1281.
- (7) Cao, Z.; Wang, L.; Zhang, H.; Zhang, X.; Liao, J.; Dong, J.; Shi, J.; Zhuang, P.; Cao, Y.; Ye, M.; Shen, J.; Ajayan, P. M. Localized Ostwald Ripening Guided Dissolution/Regrowth to Ancient Chinese Coin-Shaped VO_2 Nanoplates with Enhanced Mass Transfer for Zinc Ion Storage. *Adv. Funct. Mater.* **2020**, *30*, 2000472.
- (8) Puttaswamy, R.; Nagaraj, R.; Kulkarni, P.; Beere, H. K.; Upadhyay, S. N.; Balakrishna, R. G.; Sanna Kotrappanavar, N.; Pakhira, S.; Ghosh, D. Constructing a High-Performance Aqueous Rechargeable Zinc-Ion Battery Cathode with Self-Assembled Mat-like Packing of Intertwined Ag(I) Pre-Inserted $V_3O_7 \cdot H_2O$ Microbelts with Reduced Graphene Oxide Core. *ACS Sustain. Chem. Eng.* **2021**, *9*, 3985-3995.
- (9) Wan, F.; Zhang, L.; Dai, X.; Wang, X.; Niu, Z.; Chen, J. Aqueous Rechargeable Zinc/Sodium Vanadate Batteries with Enhanced Performance from Simultaneous

Insertion of Dual Carriers. *Nat. Commun.* **2018**, *9*, 1656.

- (10) Liu, C.; Li, R.; Liu, W.; Shen, G.; Chen, D. Chitosan-Assisted Fabrication of a Network C@V₂O₅ Cathode for High-Performance Zn-Ion Batteries. *ACS Appl. Mater. Interfaces* **2021**, *13*, 37194-37200.
- (11) Yu, X.; Hu, F.; Guo, Z. Q.; Liu, L.; Song, G. H.; Zhu, K. High-Performance Cu_{0.95}V₂O₅ Nanoflowers as Cathode Materials for Aqueous Zinc-Ion Batteries. *Rare Met.* **2022**, *41*, 29-36.
- (12) Zhu, T.; Mai, B.; Hu, P.; Liu, Z.; Cai, C.; Wang, X.; Zhou, L. Ammonium Ion and Structural Water Co-Assisted Zn²⁺ Intercalation/De-Intercalation in NH₄V₄O₁₀·0.28H₂O. *Chin. J. Chem.* **2021**, *39*, 1885-1890.
- (13) Hu, P.; Zhu, T.; Ma, J.; Cai, C.; Hu, G.; Wang, X.; Liu, Z.; Zhou, L.; Mai, L. Porous V₂O₅ Microspheres: A High-Capacity Cathode Material for Aqueous Zinc-Ion Batteries. *Chem. Commun.* **2019**, *55*, 8486-8489.